iJRASET
International Journal For Research in Applied Science and Engineering Technology

INTERNATIONAL JOURNAL FOR RESEARCH

IN APPLIED SCIENCE & ENGINEERING TECHNOLOGY

Volume: 7 **Issue:** I **Month of publication:** January 2019

DOI: http://doi.org/10.22214/ijraset.2019.1012

www.ijraset.com

Call: 08813907089 | E-mail ID: ijraset@gmail.com

International Journal for Research in Applied Science & Engineering Technology (IJRASET)
ISSN: 2321-9653; IC Value: 45.98; SJ Impact Factor: 6.887
Volume 7 Issue I, Jan 2019- Available at www.ijraset.com

Synthesis and Structural Studies of $Ce_{0.5}Sr_{0.5}(Co_{0.8}Fe_{0.2})_{1-x}Zr_xO_{3-\delta}$ (CSCFZ) Cathode Materials for IT-SOFC

Beyene Tesfaw Ayalew[1], P. Vijay Bhaskar Rao[2]
[1, 2]*Department of physics, Wollega University, Nekemte, Ethiopia*

Abstract: ***$Ce_{0.5}Sr_{0.5}(Co_{0.8}Fe_{0.2})_{1-x}Zr_xO_{3-\delta}$ (CSCFZ) powders had been synthesized by Sol-Gel method and characterized. The sintered samples were characterized using XRD, SEM with EDS, Raman spectroscopy and TGA-DTA. X-ray diffraction and scanning electron microscope observation were carried out to examine the structures and morphologies of CSCFZ samples sintered at temperature of 900°C. XRD results showed the perovskite phase with average crystallite size of 18.14, 18.13 and 18.12 for x = 01, 0.15 and 0.2 respectively. The samples were porous with porosities of 9.87%, 9.50% and 9.08%. Raman spectroscopy proved that the prepared samples were Raman active with the existence of lattice vibrations with broader peaks at five shoulders. TGA-DTA results gave information there were weight losses three times due to evaporation of moisture, evaporation of nitrates and evaporation of other impurities that comes from the usage of acids and bases.***

Keywords: XRD, SEM, Sol-Gel, Density, $Ce_{0.5}Sr_{0.5}(Co_{0.8}Fe_{0.2})_{1-x}Zr_xO_{3-\delta}$

I. INTRODUCTION

Solid oxide Fuel cell (SOFC) is an energy conversion device that converts chemical energy of fuels directly in to electrical energy with high efficiencies and minimal or zero emissions. SOFCs are an important technology for a potentially wide variety of applications. The building blocks of a fuel cell consist of an electrolyte layer in contact with a porous anode and cathode on either side [1]. To reduce the cost of SOFCs there is significant interest in lowering the operating temperature of SOFCs [2]. SOFCs are based on an O^{2-} conducting electrolyte and give a chance to use higher hydrocarbons directly without a reforming step [3]. SOFC performance powerfully depends on the electrode morphology, particle size, sintering conditions and porosity. Porosity is a typical factor of microstructure, which plays a significant role in cell performance.

Partial decomposition of the Perovskite influences the cell degradation than interface reactions during the operation [4, 5]. Since LSM show some drawbacks for low operating temperature due to poor oxygen ion conduction, $La_{1-x}Sr_xF\ eO_{3-\delta}$ had been proposed as SOFC cathode at low temperature. The microscopic mechanisms of doping effect provide deeper understanding into structure property relations [6]. Understanding fundamental aspects of oxygen self-diffusion in solid state ionic systems is important for the discovery of next-generation electrolyte and cathode material compositions and microstructure that can enable the operation of SOFCs at lower temperatures more efficiently, durably, and economically [7]. Even if the magnitudes of the electrical conductivity and thermal expansion of the $La_{0.8}Sr_{0.2}$ (Mn, F e, Co) $O_{3-\delta}$ Perovskite are mainly dependent on the percentage of Co in the compositions [8], substitution of the La cation at A-sites by Pr cation with multiple valence states can further improve the cathode performance.

Mahdi Darab [9] synthesized and characterized both $Ba_{0.5}Sr_{0.5}Co_{0.2}F\ e_{0.8}O_{3-\delta}$ and $Ba_{0.5}Sr_{0.5}Co_{0.8}F\ e_{0.2}O_{3-\delta}$, among which the second composition has shown to be promising in terms of physical properties. $Ba_{0.5}Sr_{0.5}Co_{0.8}F\ e_{0.2}O_{3-\delta}$ (BSCF5080), in which 50 percent of Sr was substituted by Ba, has reached high oxygen permeability and was estimated to be structurally stable based on the evaluation of the Goldschmidt tolerance factor and is the main composition in many following studies [10]. Although BSCF shows excellent electrochemical performance, it have high thermal expansion coefficient (TEC) with a value of $20\times10^{-6}K^{-1}$ between 50°C and 1000°C [11]. This indicates that thermal cycling could be problematic for cells using this cathode material due to a mismatched TEC with those of other cell components.

$Ba_{0.5}Sr_{0.5}Co_{0.8}F\ e_{0.2}O_{3-\delta}$ (BSCF) at 700 °C was developed by using two sintering approaches. The first was a two-step sintering process in which fine hexagonal-phase BSCF powders prepared by a novel low temperature solid state reaction before sintering. The second approach was one-step sintering process using reactive sintering which is the simultaneous reaction of BSCF from its precursors. The reactive sintered body of hexagonal-phase BSCF obtained by the one-step process showed higher electrical conductivity of $6.35Scm^{-1}$ at 500 °C than the two-step sintered BSCF of electrical conductivity $4.15Scm^{-1}$ [12]. The addition of fifth

cation at the stage of the synthesis route is one of the popular attempts to improve the performance of the cathode. Although there were many cathodes used (such as LSM, LSC, LSCF, BSCF, etc.), the thermo-mechanical suitability between electrolyte and cathode can be improved by mixing cathode material with new element or a small impurity like Zirconium, Titanium. Such composite cathode will have a better ionic conductivity and over potential of the cathode can be reduced by adding Zirconium or Titanium [13].

II. EXPERIMENTAL

Cathode materials of $Ce_{0.5}Sr_{0.5}$ $(Co_{0.8}Fe_{0.}2)_{1-x}$ $Zr_xO_{3-\delta}$ (CSCFZ) for x=0.1, 0.15 and 0.2 were synthesized by sol-gel method. AR-grade sigma-Aldrich Precursor powders of Ce $(NO_3)_3.6H_2O$, Sr (NO3)2, Co $(NO_3)_2.6H_2O$, Fe $(NO_3)_3.9H_2O$ and ZrO $(NO_3)_2.H_2O$ powders were mixed together by weighing stoichiometrically with a digital micro balance and dissolved in distilled water. Stoichiometric amount of citric acid was dissolved in the minimal amount of distilled water and mixed with the solution of metal nitrates by continuously stirring with a magnetic stirrer without heat. The solution was slowly heated for 5hrs at 80°C over a temperature controlled magnetic stirrer with a hot plate. To avoid the appearance of hydroxides and base salts at higher pH values, the pH was adjusted to ~ 7. After the pH was adjusted, heating was continued until the solution becomes a viscous like solid called gel. After the gel was formed stirring is stopped and continuing heating until it becomes a black ash. The black ashes were grinned with agate mortar continually for 1hr and small amount of powders were taken for TGA-DTA analysis to decide the sintering temperature of the samples and to study the thermal properties. The rest powders were putted in furnace for pre-sintering for 3hrs at 750 ^oC. The pre-sintered powders again grinned for 1hr with agate mortar. The powders were made pellets by adding a polyvinyl alcohol gel for binding purpose. The pellets were made by using a hydraulic press with stainless steel diset by applying a load of 12 ton for one minute. At the end, the prepared pellets were sintered at 900 ^oC for 5hrs to get the final composition and the desired pure phase Perovskites before characterization and measurements. Sintering temperature, atmosphere, heating and cooling rates, impurity concentrations and particle size had been controlled to obtain appropriate results. Since sintering process has an influence on the microstructure of the resulting ceramic, the pressed pellets were sintered in high temperature furnace with a closed alumina crucibles. The cooling rate also has a strong influence on the electrical property of the ceramics. The procedures had been repeated many times to get the highest purity crystalline phases of CSCFZ. Characterizations of the samples were carried out using X-ray Diffractometer (XRD) for crystalline phase identification, Raman spectroscopy for vibrational, rotational, and other low-frequency mode studies of the materials, Scanning electron microscopy (SEM) for surface morphology, Energy Dispersive Spectroscopy (EDS) for quantifying chemical composition at sub micron length scales and TGA-DTA for analyzing thermal properties.

III. RESULTS AND DISCUSSIONS

A. X-ray Diffractometer

X-ray diffraction had been done to study the crystalline structures of all the three samples. X-ray diffraction data were taken by Xpert Philips XRD using Cu-Kα radiation with a wave length of λ=0.1542nm at a scanning rate of 2^o/min with a Cu anode of 40kv and 30mA. Scanning was taken for 2θ values of ranging from 20 ^{o} to 80 ^{o}. From XRD patterns lattice parameters were calculated using Unit Cell Win software. The average size of particles was calculated from the peak broadening using the Scherer formula from XRD data.

$$D = \frac{0.9\lambda}{\beta \cos\theta} \quad \ldots\ldots\ldots\ldots (1)$$

Where D is the crystallite size, λ is Cu-Kα radiation wave length, β is full width half maximum and θ is diffraction angle.

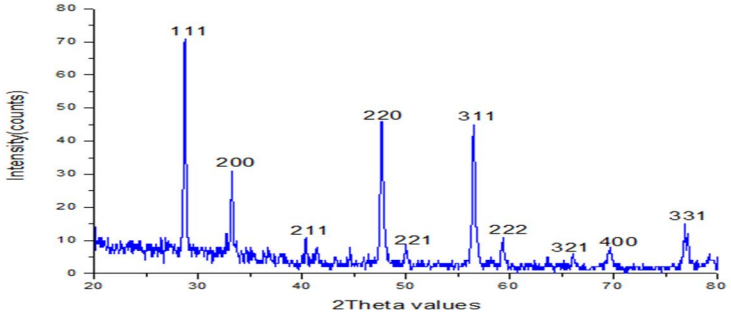

Figure 1: X-ray diffraction pattern $Ce_{0.5}Sr_{0.5}$ $(Co_{0.8}Fe_{0.}2)_{1-x}$ $Zr_xO_{3-\delta}$ sample at concentration x=0.2

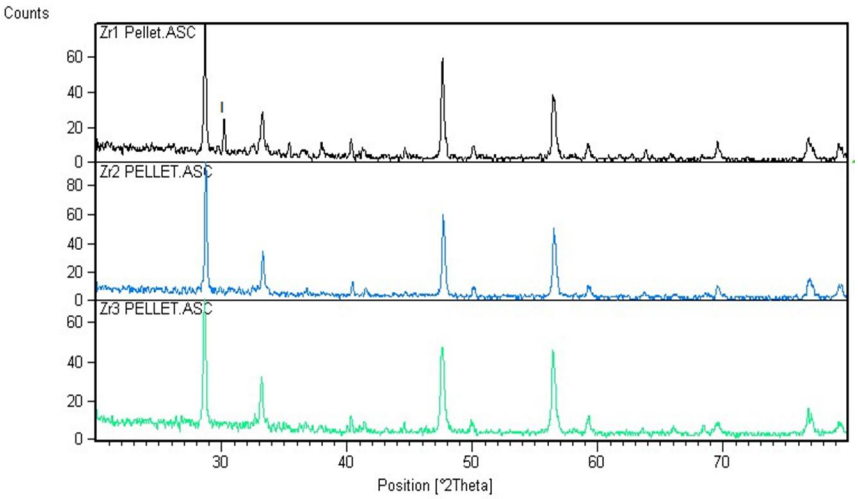

Figure 2: X-ray diffraction patterns of three samples at concentration x= 0.1, 0.15 and 0.2 from top to bottom respectively

XRD patterns confirm the presence of a single-phase Perovskite structure containing cerium doping level up to 15% in A-site. As the concentration of cerium exceeds 15%, a small peak due to un-reacted CeO_2 appears and its intensity increases with increment of cerium doping [14]. To overcome this problem zirconium is doped at B-site. As observed from figure 2, the crystalinity nature of the materials increased as the doping of Zr increases and the impurity peak (I) comes from un reacted CeO_2 uninvolved for high concentration of Zr and the sharpness of the peaks increased.

Table 1: Average crystallite size, density and lattice parameters of the prepared samples

S.name	Pos. ($2\theta^0$)	Height (cts)	FWHM ($2\theta^0$)	Average crystallite size D (nm)	Lattice constant a (Å)	Cell volume ($Å^3$)
$CeZr_1$	28.7046	61.87	0.4720	18.14	5.40527	157.9255
$CeZr_2$	28.7790	63.34	0.4723	18.13	5.40213	157.6507
$CeZr_3$	28.8054	64.20	0.4723	18.12	5.40200	157.6390

From table 1, the position of the highest intensity peak is displaced a small amount to the highest angle due to the concentration of doping Zr on B-site. The plane giving rise to the smallest Brag angle would have the highest d-spacing. The average crystallite size, lattice parameter and cell volume also decreases with the increment of fifth doping on B-site due to the shifting of the potion angle which leads to the decrement of d-spacing.

Table 2: Percentage density and porosity of prepared nano material samples

S. name	Exp. Density (gr/cm^3)	X-ray density (gr/cm^3)	Density (%)	Porosity (%)
$CeZr_1$	5.39676	5.98775	90.13	9.87
$CeZr_2$	5.38508	5.95028	90.50	9.50
$CeZr_3$	5.38427	5.92153	90.92	9.08

From table 2, the percentage density of the samples increases as partial substitution of lighter elements with heavier element increases due to the concentration of the doping element Zr on B-site. As a result the porosity of samples decreases by small amount due to doping concentration. Even if porosity is one key criterion for SOFC cathode materials, stability of the materials also play a great role on the performances of SOFCs. The stability depends on the crystalinity of the material and it was observed that the crystalline nature of the samples increased as the concentration of the fifth doping on B-site increased. But the porosity of samples was not decreased that much due to the increment of the doping concentration.

B. SEM with EDS Analysis

A high resolution SEM (ZEISS) was used to see the microstructure of the synthesized samples and to relate them with physical behaviors of the particles as a cathode material. As it is clearly seen from figures given below, the crystal consists of a periodic arrangement of the unit cell into a lattice and exhibited complete densification with a presence of pores on the surface. All samples had the required elemental composition with their proportional weight percentage.

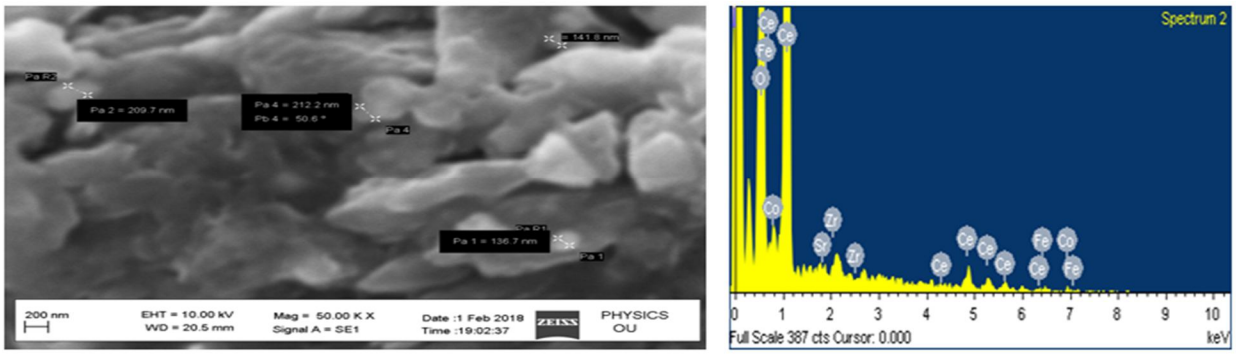

Figure 3: SEM with EDS pictures $Ce_{0.5}Sr_{0.5}(Co_{0.8}Fe_{0.2})_{1-x}Zr_xO_{3-\delta}$ sample for x=0.1

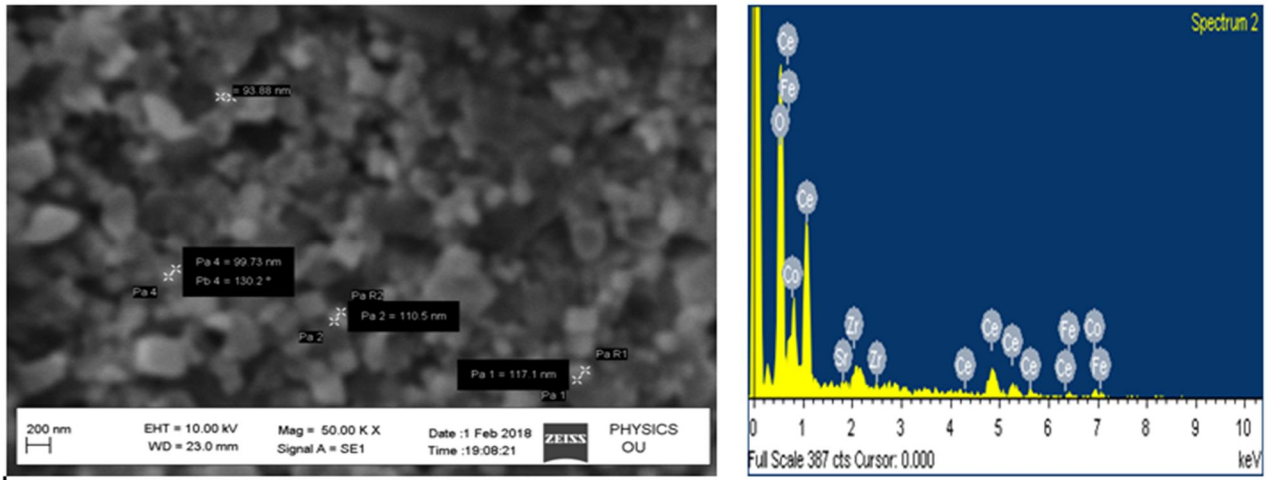

Figure 4: SEM with EDS pictures $Ce_{0.5}Sr_{0.5}(Co_{0.8}Fe_{0.2})_{1-x}Zr_xO_{3-\delta}$ sample for x=0.15

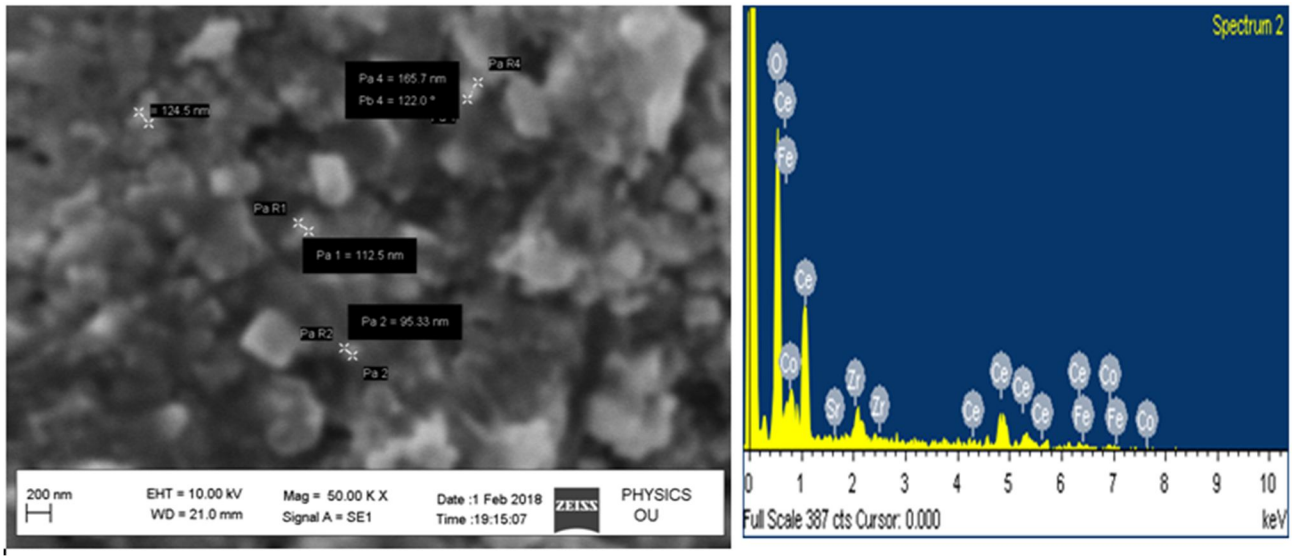

Figure 5: SEM with EDS pictures $Ce_{0.5}Sr_{0.5}(Co_{0.8}Fe_{0.2})_{1-x}Zr_xO_{3-\delta}$ sample for x=0.2

C. Raman Spectroscopy Analysis

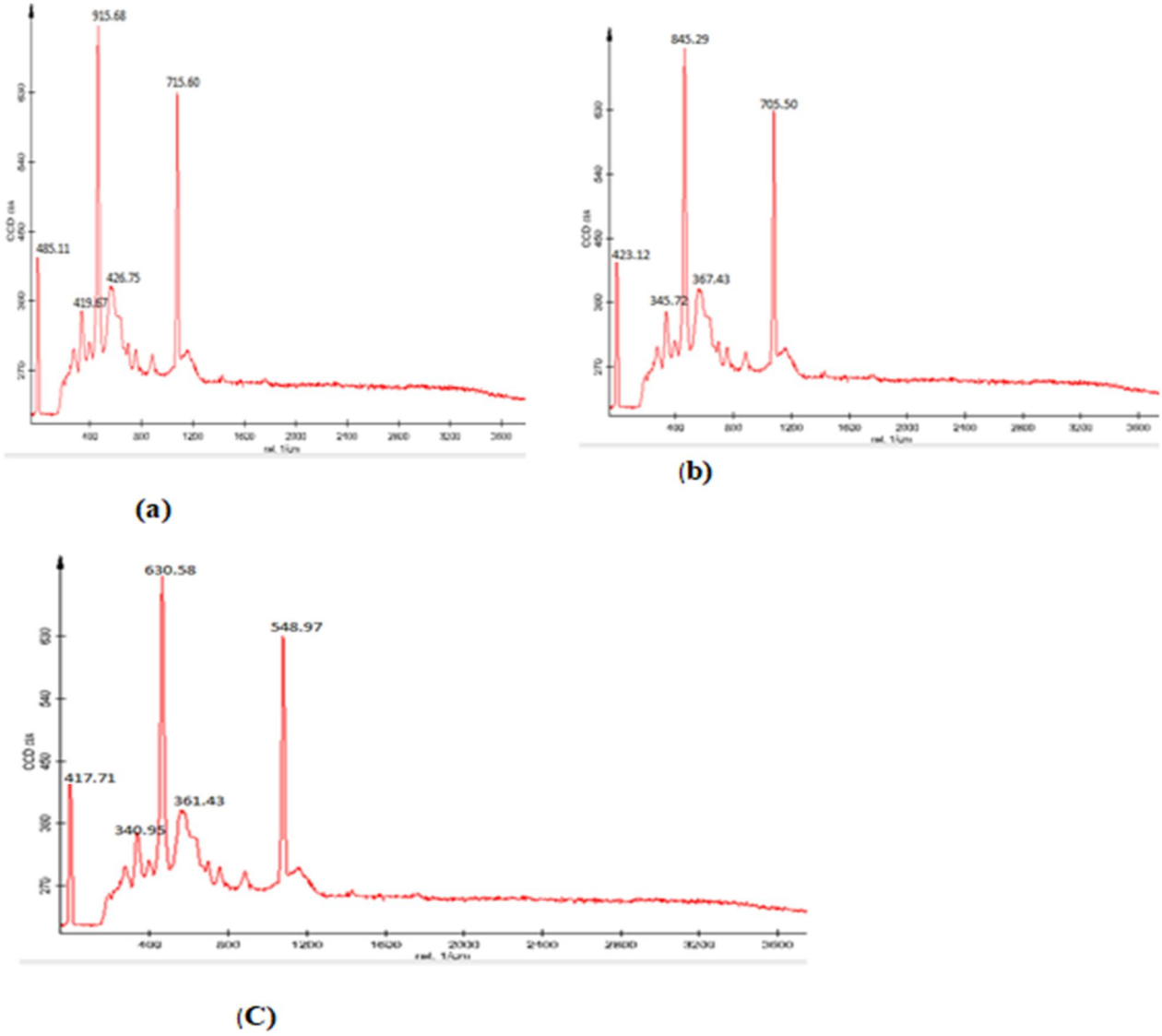

Figure 6: Raman spectra of $Ce_{0.5}Sr_{0.5}(Co_{0.8}Fe_{0.2})_{1-x}Zr_xO_{3-\delta}$ samples (a) for x=0.1, (b) for x=0.15 and (c) for x=0.2 for SOFC cathode materials

Raman spectroscopy is capable to distinguish the amorphous and crystalline state of materials much more precisely than the x-ray diffraction [15]. As it was seen from figure 6, the samples were Raman-active and exhibits five peaks. The peaks are broader and contain a shoulder. A perfect cubic Perovskite has no Raman active phases. Since the samples were Raman active as seen from the figures there were a distortion in crystal structures and oxygen vacancies were formed due to doping. As it is clearly observe from figure 6, the values of shoulders are decreased as the concentration of Zr doping increased resulted to the decrement of oxygen vacancies. These decrement of oxygen vacancies told information about perfect cubic Perovskites would be formed as the concentration of the fifth doping increased much more.

D. Results of TGA-DTA Analysis

TGA-DTA is performed to determine changes in weight in relation to change in temperature. The synthesized samples are placed on the platinum pan that is suspended from the analytical balance located outside the furnace chamber of the instrument TGA Q500 V20.13Build 39. The balance is zeroed and the sample cup is heated up from room temperature to 800°C. Powders of 3.5880mg, 3.0910mg and 3.0650mg were taken and corresponding curves were recorded for $Ce_{0.5}Sr_{0.5}(Co_{0.8}Fe_{0.2})_{1-x}Zr_xO_{3-\delta}$ (CSCFZ) for x=0.1, 0.15 and 0.2 respectively.

ISSN: 2321-9653; IC Value: 45.98; SJ Impact Factor: 6.887
Volume 7 Issue I, Jan 2019- Available at www.ijraset.com

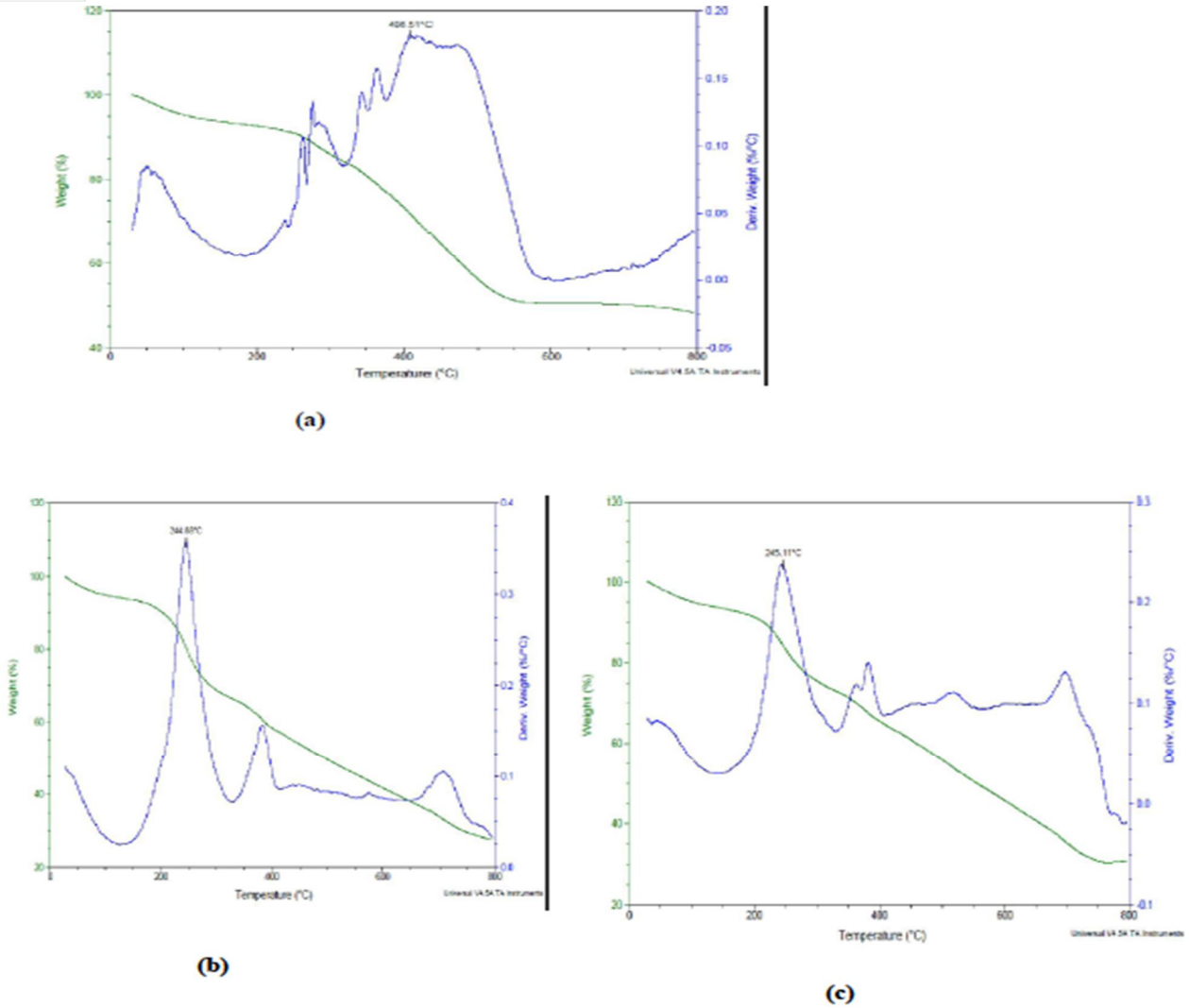

Figure 7: Thermo gravimetric (TGA-DTA) analysis for CSCFZ samples; (a) for x=0.1, (b) for x=0.15 and (c) for x=0.2

The TGA curve calculations of samples on this study indicated that the decomposition of calcite occurred at lower temperature. The weight loss is observed three times in the curve [16]. As it is observed from figure 7, the weight loss is observed three times in the curve for all three samples. First it was at due to evaporation of moisture, second at due to evaporation of nitrates and the third at due to evaporation of other impurities that comes from the usage of acids and bases.

IV. CONCLUSIONS

All powders were synthesized by Sol-Gel method and characterized their structural properties. XRD pattern of the samples were taken and the crystalinity nature of the sample observed and nano sized particles for all samples. SEM with EDS images show the presence of porosity and elemental composition respectively in the samples. The vibrational modes of the molecules or the lattice phonon modes of a crystal were analyzed using Raman spectroscopy and showed that the materials are Raman active with five shoulders. The changes of weight in relation to change in temperature for the three samples were done using TGA-DTA. The pre-sintering and final sintering temperatures of the samples were also decided using the results got from TGA-DTA.

V. ACKNOWLEDGEMENTS

The authors would like to express their gratitude to department of physics and chemistry of Osmania University and central university Hyderabad for allowing to use their laboratory facilities. Finally, we would like to thank ministry of finance of Ethiopia for funding this work.

REFERENCES

[1] Stefen S. (2014). Yttria-stablized zerconia and gadolinia-doped ceria thin films for fuel cell applications. 0345-7524.
[2] Ormerod, R. M. (2003). Solid oxide fuel cells. Chemical Society Reviews, 32, 17-28.
[3] McIntosh, S., & Gorte, R. J. (2004). Direct hydrocarbon solid oxide fuel cells. American Chemical Society, 104, 4845-4865.
[4] Tietz, F., Fu, Q., Haanappel, V., Mai, A., Menzler, N., & Uhlenbruck, S. (2007). Materials Development for Advanced Planar Solid Oxide Fuel Cells. Applied Ceramic Technology, 4, 436.
[5] Yokokawa, H., Tu, H., Iwanschitz, B., & Mai, A. (2008). Fundamental mechanisms limiting solid oxide fuel cell durability. Journal of Power Sources, 182, 400-412.
[6] Sora, I. N., Felice, V., & Fontana, F. (2015). Structural Studies of Doped Lanthanum Orthoferrites of Interest for SOFCs. Italian Association of Chemical Engineering, 43.
[7] Chroneos, A., Yildiz, B., Tarancon, A., Parfitt, D., & Kilner, J. A. (2011). Oxygen diffusion in solid oxide fuel cell cathode and electrolyte materials: mechanistic insights from atomistic simulations. Energy Environ. Sci., 4, 2774.
[8] Tietz, F., Mai, A., & Stöver, D. (2008). From powder properties to fuel cell performance-A holistic approach for SOFC cathode development. Solid State Ionics, 179, 1509-1515.
[9] Darab, M. (2008). Synthesis and Characterization of nanostructured Cathode Material (BSCF) for Solid Oxide Fuel Cells. 20-50.
[10] Shao, Z. P., Yang, W. S., Cong, Y., Dong, H., Tong, J. H., & Xiong, G. X. (2001). Operation of perovskite membrane under vacuum and elevated pressures for high-purity oxygen production. Membrane Science, 345, 47-52.
[11] Wei, B., Lü, Z., Huang, X., Miao, J., Sha, X., Xin, X., et al. (2006). Crystal structure, thermal expansion and electrical conductivity of perovskite oxides $Ba_xSr_{1-x}Co_{0.8}F e_{0.2}O_{3-\delta}$ ($0.3 \leq x \leq 0.7$). Journal of the European Ceramic Society, 26, 2827-2832.
[12] Yamaguchi, Y., Sumi, H., Shimada, H., Yamaguchi, T., & Nomura, K. (2017). Reactive-sintering of $Ba_{0.5}Sr_{0.5}Co_{0.8}Fe_{0.2}O_{3-\delta}$ using alkaline earth peroxides for low-temperature synthesis. Journal of the Ceramic Society of Japan, 125, 681-685.
[13] Sharma, D. R., Rao, P. V., Reddy, M. N., & Srikanth, D. (2015). Synthesis and Characterization of $Ba_{0.5}Sr_{0.5}(Co_{0.8}F e_{0.2})_{1-x}Zr_xO_{3-\delta}$ (BSCF) Nanoceramic Cathode Powders by Sol-Gel Process for Solid Oxide Fuel Cell. Materials Today: Proceedings, 2, 4442-4450.
[14] Choi, H., Fuller, A., Davis, J., Wielgus, C., & Ozkan, U. S. (2012). Ce-doped strontium cobalt ferrite perovskites as cathode catalysts for solid oxide fuel cells: Effect of dopant concentration. Applied Catalysis B: Environmental, 127, 336- 341.
[15] Cavallaro, A., Pramana, S. S., Ruiz-Trejo, E., Sherrell, P. C., Ware, E., Kilner, J. A., et al. (2018). Amorphous-cathode-route towards low temperature SOFC. Sustainable Energy & Fuels, 4-6.
[16] Sharma, D. R., & Rao, D. P. (2015). Synthesis and characterization of $Ba_{0.5}Sr_{0.5}(Co_{0.8}F e_{0.2})_{1-x}Ti_xO_{3-\delta}$ (BSCF) cathode for solid oxide fuel cell. International Journal of Scientific and Research Publications, 5, 6-7.

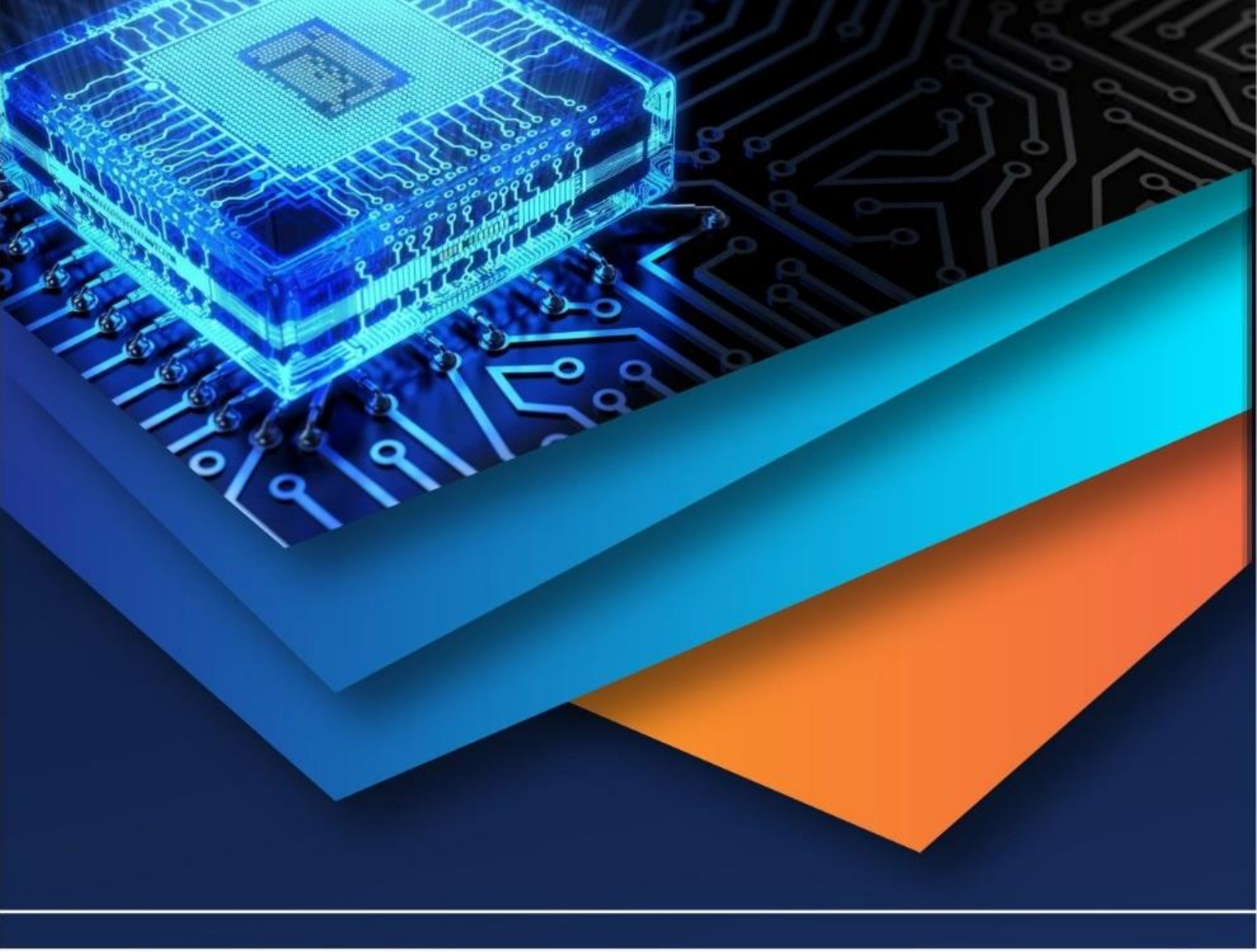

10.22214/IJRASET

45.98

IMPACT FACTOR: 7.129

IMPACT FACTOR: 7.429

INTERNATIONAL JOURNAL FOR RESEARCH

IN APPLIED SCIENCE & ENGINEERING TECHNOLOGY